

Genome-guided discovery of natural products through multiplexed low coverage whole-genome sequencing of soil Actinomycetes on Oxford Nanopore Flongle

Rahim Rajwani¹, Shannon I. Ohlemacher¹, Gengxiang Zhao¹, Hong-bing Liu¹, Carole A. Bewley^{1#}

¹ Laboratory of Bioorganic Chemistry, National Institute of Diabetes and Digestive and Kidney Diseases, National Institutes of Health, Bethesda, Maryland 20892, United States

Correspondence to Dr. Carole A. Bewley (caroleb@nih.gov)

1 Abstract

2

3 Genome-mining is an important tool for discovery of new natural products; however, the number of
4 publicly available genomes for natural product-rich microbes such as Actinomycetes, relative to human
5 pathogens with smaller genomes, is small. To obtain contiguous DNA assemblies and identify large (ca.
6 10 to greater than 100 Kb) biosynthetic gene clusters (BGCs) with high-GC (>70%) and -repeat content, it
7 is necessary to use long-read sequencing methods when sequencing Actinomycete genomes. One of the
8 hurdles to long-read sequencing is the higher cost.

9 In the current study, we assessed Flongle, a recently launched platform by Oxford Nanopore
10 Technologies, as a low-cost DNA sequencing option to obtain contiguous DNA assemblies and analyze
11 BGCs. To make the workflow more cost-effective, we multiplexed up to four samples in a single Flongle
12 sequencing experiment while expecting low-sequencing coverage per sample. We hypothesized that
13 contiguous DNA assemblies might enable analysis of BGCs even at low sequencing depth. To assess the
14 value of these assemblies, we collected high-resolution mass-spectrometry data and conducted a multi-
15 omics analysis to connect BGCs to secondary metabolites.

16 In total, we assembled genomes for 20 distinct strains across seven sequencing experiments. In each
17 experiment, 50% of the bases were in reads longer than 10 Kb, which facilitated the assembly of reads
18 into contigs with an average N50 value of 3.5 Mb. The programs antiSMASH and PRISM predicted 629
19 and 295 BGCs, respectively. We connected BGCs to metabolites for *N,N*-dimethyl cyclic-ditryptophan, a
20 novel lasso peptide and three known Actinomycete-associated siderophores, namely mirubactin,
21 heterobactin and salinichelin.

22 Importance

23 Short-read sequencing of GC-rich genomes such as Actinomycetes results in a fragmented genome
24 assembly and truncated biosynthetic gene clusters (often 10 to >100 Kb long), which hinders our ability
25 to understand the biosynthetic potential of a given strain and predict the molecules that can be
26 produced. The current study demonstrates that contiguous DNA assemblies, suitable for analysis of
27 BGCs, can be obtained through low-coverage, multiplexed sequencing on Flongle, which provides a new
28 low-cost workflow (\$30-40 per strain) for sequencing Actinomycete strain libraries.

29 Introduction

30

31 Clinical pathogens are increasingly becoming resistant to currently used antimicrobials causing over
32 700,000 deaths worldwide (1). New antimicrobials are urgently needed to alleviate antimicrobial
33 resistance and prevent deaths per year to rise over 10 million by 2050 (1). One of the prolific sources of
34 new antimicrobials is a group of gram-positive mycelia forming bacteria, the Actinomycetes. Several
35 currently used antibiotics, including vancomycin, rifamycin, and streptomycin are isolated from
36 Actinomycetes and they still hold enormous potential for the future discovery of new medicines (2).

37 Genome sequencing is now an important component of natural products research. Whole-genome
38 sequencing (WGS) enables identification of the genes responsible for the biosynthesis of natural
39 products (3). Often genes required for the biosynthesis of a natural product positionally cluster on the
40 genome and are referred to as biosynthetic gene clusters (BGCs) (4). The BGC sequences can be used to
41 predict possible structures of the resulting natural product (5), assess novelty of the compound (6) and
42 dereplicate compounds from a strain collection (7). Despite the merits offered by WGS, the number of
43 Actinomycete genomes remains limited. Several rare genera are not represented by a complete
44 genome, and the majority of currently available genomes are sequenced using Illumina short-read
45 technology that results in highly fragmented assemblies. BGCs span multiple contigs in fragmented
46 genome assemblies and cannot be detected or analyzed by commonly used BGC prediction tools such as
47 antiSMASH (8, 9).

48 Long-read sequencing technologies (e.g. PacBio or Oxford Nanopore Technologies, ONT) produce
49 contiguous genome sequences needed to analyze secondary metabolite gene clusters. Notably, PacBio
50 assemblies achieve consensus accuracy over 99.999%; however, it is generally less accessible due to the
51 upfront cost of sequencing instruments and higher per sample sequencing costs. By contrast, ONT does
52 not require an upfront cost of an expensive sequencing instrument and the devices are inexpensive.
53 Nevertheless, ONT data results in a lower consensus accuracy (99.9%) and often requires polishing with
54 Illumina reads to obtain reference-quality genomes. We hypothesized that while BGC identification
55 requires a contiguous DNA sequence, it might be less affected by the lower consensus accuracy of a
56 Nanopore assembly since most BGC analysis steps involve inferring homology between distantly related
57 amino acid sequences using profile Hidden Markov models. If this is true, contiguous DNA assemblies
58 can be obtained at ca. 10x coverage using ONT, allowing complete genome sequencing at a significantly
59 lower cost. While such ONT sequenced genomes would still require error correction with Illumina reads,
60 they could be used on their own to sequence a strain collection, build a catalog and compare BGCs for
61 dereplication or identification of potentially new compounds, which might be particularly useful to
62 natural product research and drug discovery programs.

63 To assess the feasibility of obtaining contiguous assemblies from ca. 10x sequencing depth, predicting
64 BGCs, and connecting BGCs to metabolites, we conducted the current multi-omics study. We sequenced
65 20 new soil-derived Actinomycete strains and analyzed their metabolome using high-resolution mass
66 spectrometry (HRMS). For sequencing, we specifically selected Flongle, a recently launched ONT
67 sequencing device that costs \$90 USD and can generate up to 1-2 Gigabases of sequence output. With a
68 typical Actinomycetes genome being 8-10 Mb, a single Flongle experiment might be sufficient to
69 sequence 3-4 strains at 20-30x coverage. Sequencing workflows based on Flongle could be broadly
70 applicable to small and large studies due to the modular experimental design. In the current study, we

71 obtained 300-850 Mb of data per experiment across ten sequencing experiments with read-length N50
72 values over 10 Kb. Assembling of reads resulted in contiguous assemblies (average contig N50 value =
73 3.5 Mb and average number of contigs = 47.3). AntiSMASH5 predicted a total of 629 BGCs from these
74 assemblies. Through a combined analysis with metabolomics data, we were able to connect BGCs to
75 their secondary metabolites. The study demonstrates the utility of low coverage nanopore-only
76 assemblies as a rapid and low-cost sequencing option to advance natural product research.

77 Results

78 [An in silico analysis to study the effect of sequencing coverage and read length on BGC](#) 79 [detection](#)

80 We first analyzed what level of sequencing coverage would be sufficient for contiguous assemblies and
81 BGC detection using Oxford Nanopore sequencing. For this purpose, three Actinomycete genomes,
82 previously sequenced at high coverage, were downloaded from the European Nucleotide Archive and
83 their reads were down sampled to 60x, 30x, 15x and 7x coverage (assuming a genome size of 8 Mb)
84 before assembling and detecting BGCs. While actual genome sizes of the three genomes differed (Table
85 S 1), an assumption of a fixed expected genome size of 8 Mb allowed us to determine the utility of a
86 prospective sequencing experiment where Actinomycete genome sizes would not be known. In the
87 down sampling analysis, assembly size and number of predicted genes nearly plateau at ca. 15x
88 coverage. Similarly, a sharp decline in the number of contigs and number of mismatches per 100 Kb was
89 observed at ca. 15-20x coverage (Figure 1). At approximately the same coverage of 15-20x, 72-96% of
90 BGCs were detected by antiSMASH and a further increase in coverage led to detection of only 1-6
91 additional BGCs (Figure 1). Moreover, most of the BGCs were not located at the edge of a contig, also
92 referred to as complete. Relative to antiSMASH, PRISM predicted a lower number of BGCs. This could be
93 because antiSMASH was run in a 'relaxed' mode in this study whereas PRISM does not have this option.
94 Nevertheless, the trend relative to coverage was similar between antiSMASH and PRISM.

95 Assembly contiguity and therefore BGC detection in a Nanopore sequencing experiment is also related
96 to read length. In another computational experiment, we evaluated whether longer reads might enable
97 a more contiguous DNA assembly and BGC detection at fixed coverage. For this purpose, simulated
98 Nanopore reads of average length 500, 1000, 2000 and 4000 were generated at 10x coverage of a
99 *Streptomyces* genome (GB4-14) using BadRead. The resulting reads were assembled and analyzed for
100 assembly contiguity and BGC detection. It was observed that an ca. 2-fold increase in average read
101 length was associated with a 2-fold reduction in the number of contigs (Figure S 3). Improved assembly
102 contiguity also led to a reduction in the number of BGCs on contig edges (incomplete) and an increased
103 number of complete BGCs with little to no change of sequencing coverage (Figure S 4).

104 Overall, these computational experiments suggested contiguous DNA assemblies and complete BGCs
105 can be detected at low sequencing coverage using long reads from Oxford Nanopore Technologies; this
106 should allow for a dramatic reduction in cost per genome through multiplexing. The computational
107 experiments were followed up with prospective sequencing of Actinomycetes genomes using Flongle
108 and more detailed analyses of BGCs described in the following sections.

109 Nanopore sequencing, genome assembly and quality assessment

110 A total of ten sequencing experiments were conducted— each with an attempt to sequence four
111 Actinomycetes strains (Figure 2). Impurities in the starting genomic DNA (as measured by a ratio of the
112 UV absorbance at 260 and 280nm) and low pore occupancy (caused by insufficient loading of the library
113 or inhibition of adapter ligation) resulted in three unsuccessful experiments with a total output <100
114 megabases (Mb) per experiment. The remaining seven experiments yielded 288- 797 Mb over 18-24
115 hours. The longest read for each sample was over 80 Kb.

116 Across the experiments, we tried different buffers for bead-based purification to apply size selection and
117 increase the read length N50 values from standard protocols (Table S 2) (Figure 2). One of our initial
118 experiments using 0.5x of the standard buffer concentration was not successful resulting in read N50
119 values of 1-1.6 Kb for three out of five samples sequenced in the experiment. In two subsequent
120 successful experiments (AET670 and AFK704), we utilized 0.15x of a modified buffer containing 0.5 M
121 MgCl₂ + 5% PEG in TE buffer (10 mM Tris-Cl pH 8.0, 1 mM EDTA) for bead-based purification after
122 barcodes ligation as described previously (10). Read length N50 values in these experiments were 11.6-
123 15.1 Kb (Figure 2). In three experiments (AEZ324, AFA498 and AFA876), the concentration of the
124 modified buffer-based size selection was reduced to 0.1x which led to a further increase in read length
125 N50s (10.5-23.3 Kb) accompanied by an increased sample loss. Application of size selection after
126 barcodes ligation ensures approximately equal fragment lengths for pooling of samples and adapter
127 ligation. However, ligation of barcodes could be less efficient to longer fragments if shorter fragments
128 are present in the mixture. We tested buffer-based size selection (0.1x beads in modified buffer) before
129 barcode ligation in later experiments (flow cell ids AFK426 and AFK406) (Table S 2). A more consistent
130 output was observed, possibly due to more efficient barcode/adaptor ligation to longer DNA fragments.

131 Across the seven successful runs, 3,814,434,062 bases in 751,459 reads were generated. Upon
132 demultiplexing, the median number of bases per sample was 77.5 Mb (theoretical coverage of 9.5x with
133 an expected 8 Mb genome size). Three strains were sequenced at <2.5x theoretical coverage (<20Mb
134 per strain) and were excluded from further analysis. Subsequently, 25 samples (20 distinct isolates) were
135 de novo assembled with Canu and polished with Racon and medaka (Figure 3). The median length of the
136 obtained assemblies was 8.5 Mb (average: 7.9 Mb, maximum: 9.4 Mb), typical of Actinomycete genome
137 size. The only exception was a 3 Mb assembly for GB8-002 which was also sequenced at the least
138 coverage (4.0x) (Figure 3).

139 We assessed the accuracy and quality of these low coverage genomes by comparing them with genomes
140 sequenced at high coverage on MinION or PacBio. In particular, two strains, GA3-008 and GB4-14 were
141 previously sequenced by our lab at 10-fold higher coverage using MinION and PacBio, respectively
142 (Table 1). Despite the lower sequence coverage, the genomes' contiguity was only slightly affected on
143 flongle and all were assembled into <10 contigs. The size of the assembly differed by 6.1 Kb (GA3-008)
144 and 19.6 Kb (GB4-14) due to insertion/deletion (indel) errors. Despite many mismatches and indel
145 errors, 87.5-100% of the BGCs detected in the MinION or PacBio assemblies were also detected in these
146 Flongle assemblies by antiSMASH.

147 Taxonomy and BGCs

148 antiSMASH predicted 629 BGCs of 29 different types across all assembled genomes from this study
149 (Figure S 5). Seventy-nine percent (497/629) of these BGCs were complete (i.e. not located on a contig

150 edge). There was a median of 23 BGCs per strain. The number of non-ribosomal peptide synthases
151 (NRPSs) and terpenes detected were 2-3 times greater overall than other BGC types; however, this may
152 be because antiSMASH does not subdivide these BGC types into defined sub-classifications, like it does
153 for the RiPPs (LAP, lanthipeptide, etc.) and PKS (type I, II, etc.) categories. In addition to antiSMASH, 295
154 BGCs were predicted using PRISM software. A unique feature of PRISM is that it enables chemical
155 structure prediction from BGCs (11). In the current dataset, PRISM generated a predicted chemical
156 structure for 180 out of 295 predicted BGCs.

157 The taxonomic identification based on 16S rRNA sequences extracted from the WGS revealed that the
158 dataset comprises 11 different Actinomycete species belonging to four genera (Table S 3). It consisted of
159 eight *Amycolatopsis*, nine *Streptomyces*, four *Lentzea* and four *Nocardia* species. Some species were
160 overrepresented in the dataset. *Amycolatopsis lurida* and *Streptomyces tendae* were each represented
161 with four strains and *Lentzea violacea* with two strains (Table S 3). The biosynthetic diversity between
162 strains was high with members of the same species, sharing >99% identity in their 16S sequences,
163 differing by up to 20 BGCs (Figure S 6). The biosynthetic diversity of BGCs within species also varied in
164 some cases. For instance, strains of *Streptomyces tendae*, *Lentzea violacea* or *Streptomyces*
165 *kanamyceticus* were more diverse within the species than strains of *Amycolatopsis lurida*. Different
166 species of the same genus also encoded 10-15 different BGCs on average.

167

168 Predicting metabolites from BGCs – paired analysis of genome and secondary 169 metabolites

170 Insilco PRISM-predicted chemical structures

171 The PRISM predicted BGCs detected from low coverage assemblies were analyzed further to determine
172 whether they could be linked to a metabolite. We conducted a paired analysis by collecting MS/MS
173 spectra for extracts from strain cultures grown in ISP1 and R2A media. MS/MS spectra were queried
174 using molDiscovery against a database of PRISM predicted chemical structures from BGCs (12). The
175 database comprised 1,177 structures generated from 180 BGCs sequenced in this study. A total of 18
176 predicted structures matched to MS/MS spectra collected from the strains at false discovery rate (FDR)
177 < 1% and p-value < e^{-10} . Three of these matches were also detected in media blanks and were excluded
178 from the analysis. These three metabolites corresponded to tryptophan, and the dipeptides Pro-Val and
179 Phe-Val.

180 Two of eighteen matched structures were predicted from a cyclic dipeptide BGC in *Amycolatopsis* strain
181 GA6-002 and were detected in metabolite extracts from the same strain (Figure 4). The two gene BGC
182 encoded a cyclic dipeptide synthase (CDPS) and an *N*-methyl transferase. Both of the amino acyl tRNA
183 binding pockets of the CDPS had a specificity signature for tryptophan tRNA. Based on sequence
184 information, cyclic-di-tryptophan c(WW) was predicted as a possible metabolite that can be methylated
185 on nitrogen by the *N*-methyl transferase as reported previously for *Actinosynnema mirum* (13). In all
186 chemical extracts from GA6-002, a metabolite matching the precursor *m/z* and predicted MS/MS
187 fragmentation pattern for c(WW) was detected. In addition, in the ethyl acetate extracts from ISP1
188 cultures the *N*-methylated metabolite c(WW)Me₂ was also detected.

189 An additional mass spectral match was detected for a small, glycosylated polyketide in GB4-14
190 consisting of a propionate unit and an actinosamine sugar moiety (Figure S 7), resembling a putative
191 shunt product of a larger polyketide. The corresponding BGC includes additional PKS modules that were
192 not accounted for in the structure predicted by PRISM. More complex structures that better resemble
193 final products of PKS pathways were predicted from a more contiguous Flongle (Figure 3) or PacBio
194 assembly (Table 1) of the same strain but were not detected in the metabolite extracts. The final
195 product of this BGC, predicted from PacBio sequenced genome, was therefore regarded as not detected.

196

197 RiPPs

198 We conducted a second analysis to query MS/MS spectra for post-translationally modified precursor
199 peptides from RiPPs using MetaMiner (14). All open reading frames shorter than 600 nt were extracted
200 from 43 antiSmash predicted RiPP BGCs (16 lanthipeptide, 4 LAP, 13 lassopeptides, 10 thiopeptides) and
201 included in this analysis (Figure S 5). We observed a single high confident match for a class-II
202 lassopeptide BGC in the *Amycolatopsis* sp. GA6-002 (Figure 5). The BGC encoded all essential elements
203 for lasso peptide biosynthesis including precursor peptide, asparagine synthetase (SMCOG1177 -
204 essential for macrolactam formation), lassopeptide transglutaminase protease (PF13471 - leader peptide
205 cleavage) RiPP recognition element (PF05402), and ABC transporter (SMCOG1288 and SMCOG1000) (15,
206 16)(Figure 5) [14, 15]. The precursor m/z (1041.504 $[M+2H]^{2+}$ and 694.672 $[M+2H]^{3+}$) of the matched
207 spectra was consistent with the predicted core peptide after loss of one water molecule (-18.010). The
208 MS^2 fragmentation pattern further indicated abundant ions matching m/z for y_6 and y_7 ions. The 16
209 amino acid core peptide sequence (GYPWWDNRDIFGGRTFL) is a novel lassopeptide variant with 76%
210 amino acid identity to propeptin, an endopeptidase inhibitor (17). The analysis was also repeated for
211 RiPP BGCs predicted by PRISM and no matches were detected with p-value lower than e^{-10} .

212 Known metabolites and their BGCs

213 An important application of genome sequencing is to understand the biosynthesis of known natural
214 products. Similarity to characterized BGCs can also be used for strain dereplication. To assess this
215 application on the current sequencing data, we screened MS/MS spectra for known natural products in
216 the Natural Product Atlas database (3) (29,006 compounds) using molDiscovery (12). Subsequently, we
217 analyzed genome sequences to confirm the presence of the corresponding BGCs. A total 324 significant
218 matches to known compounds were detected (p-value < e^{10}). Of these, 30 had a reference MS/MS
219 spectrum available in GNPS. We compared the spectra observed in our dataset to the reference spectra
220 available in GNPS and found highly similar MS/MS spectra (Figure S 8).

221 Twenty-one of the 324 identified compounds had a previously characterized BGC in the MiBiG database
222 (4). Twelve of these were known Actinomycete natural products; therefore, a higher sequence similarity
223 could be expected. The other nine were compounds isolated from diverse bacterial genera, including
224 those from Gram-negative bacteria and the phylum Cyanobacteria. The presence in our genomes of
225 homologous BGCs for four known Actinomycetes compounds could be confirmed using BLAST sequence
226 similarity searches (Figure 6). These compounds included *N*-acetyl tryptophan and the siderophores
227 heterobactin A, mirubactin and salinichelin. From the BGC comparisons illustrated in Figure 6, it is
228 evident that the nanopore-sequenced genomes from this study can have sequencing artifacts resulting
229 in fragmentation of large genes into multiple small ORFs (see for example the comparison of

230 mirubactin). However, matches to homologous BGCs in MiBiG were easily identified by the high
231 sequence identity between genes, shared functions, and synteny.

232

233 [BGCs encoding known antibiotic classes with no metabolites detected - glycopeptide,](#)
234 [aminoglycoside and aminocoumarin](#)

235 In addition to the above-described BGCs whose metabolites were expressed and detected by HRMS/MS,
236 many other BGCs with sequence homology to known antibiotic BGCs were also identified in the
237 sequencing data. However, we were unable to assign metabolite products to these BGCs by LC-
238 HRMS/MS data. A few such BGCs are described below.

239 Three *Amycolatopsis lurida* strains (GB15-009, GA10-003 and GA10-004) harbored a nearly identical
240 aminocyclitol gene cluster which encoded a homolog of 2-epi-5-epi-valiolone synthase (salQ)
241 responsible for the first step in the biosynthesis of C7N-aminocyclitols (18) (Figure S 9). Aminocyclitols
242 are biosynthesized from sugars through cyclization by a Sugar Phosphate Cyclase (SPC) such as
243 dehydroquinase (DHQ) synthase. The BGCs were highly homologous to cetoniacytone A sharing 70-82%
244 amino acid identity for core biosynthetic genes (19, 20).

245 In *Amycolatopsis coloradensis* B06-03, an aminocoumarin BGC was detected (Figure S 10).
246 Aminocoumarin antibiotics are biosynthesized from L-tyrosine (21). Tyrosine is activated by an
247 adenylation domain and covalently attached to a peptidyl carrier protein (PCP). A NovH-like
248 cytochrome P450 hydroxylates PCP-bound tyrosine to β -hydroxy tyrosyl-S-PCP. A 3-oxoacyl-
249 acylcarrierprotein (ACP) reductase converts it to a β -keto-tyrosyl intermediate that undergoes
250 cyclization to form 3-amino-4,7-dihydroxycoumarin. In B06-03, downstream core aminocoumarin
251 biosynthesis genes, a type-I polyketide BGC encoding co-enzyme A ligase (CAL) domain specific for 3-
252 amino-5-hydroxybenzoic acid (AHBA), was present as in rubradirin (22) and chaxamycin (23).

253 A total of seven BGCs similar to previously characterized glycopeptide BGCs were detected (Figure S 11).
254 Glycopeptides are biosynthesized through a multi-modular NRPS assembly line. Glycopeptide BGCs
255 encode additional tailoring enzymes such as P450 monooxygenases and glycosyltransferases that result in
256 amino acid crosslinking and glycosylation respectively, to yield the complex multicyclic antibiotics
257 exemplified by vancomycin. The expected glycopeptides from four glycopeptide-like BGCs (from strains
258 GA10-004, GA10-003, GB8-002, GB15-009) were similar in amino acid composition to ristocetin (24).
259 These four strains primarily contained butylated hydroxytoluene (Bht), dihydroxyphenylglycine (Dhpg)
260 and 4-hydroxyphenylglycine (Hpg) as seen in ristocetin. The predicted glycopeptide from B06-03 is
261 predicted to contain Trp, Hpg and Tyr as seen in complestatin (25).

262

263 Discussion

264

265 Soil Actinomycetes hold enormous potential for the discovery of new antibiotics. However, the number
266 of genome-sequenced Actinomycetes in the public domain is still limited, partly due to the cost of long-
267 read next-generation sequencing. In this study, we assessed the capability of the ONT Flongle platform
268 as a low-cost sequencing option to obtain multiple near-complete genomes of Actinomycetes, identify
269 BGCs, and connect them to metabolites through a paired genome-metabolome analysis.

270 Our sequencing and assembly results showed that up to four near-complete genomes of Actinomycete
271 strains could be sequenced on a single Flongle device. Skipping an optional DNA fragmentation step
272 enabled read lengths up to 80 Kb in each sample. Bead-based size selection further depleted shorter
273 DNA fragments, and enriched sequencing reads in longer sequences (10 Kb+). The long reads enabled
274 contiguous DNA assemblies at lower sequencing depth. The size of the assembly was typical of soil
275 Actinomycetes, suggesting that assemblies represent near-complete genomes of the strains. There were
276 several mismatches in the accuracy comparison analysis in flongle genomes relative to PacBio or high-
277 coverage MinION genomes. However, the contiguity of the genomes was only slightly affected (1-2
278 contigs verses 6-7 contigs), indicating that important structural information about the genome (e.g.,
279 position and organization of genes) can be inferred from these sequences.

280 A common strategy to obtain contiguous and accurate genome assemblies is through polishing
281 contiguous nanopore assemblies with Illumina reads. One of the significant findings of this study is that
282 BGC predictions and their connection to metabolites was performed without the need for error-
283 correction using Illumina reads. Based on down sampling analysis of public datasets, it was initially
284 hypothesized that low-coverage nanopore-only assemblies could be used to predict and analyze BGCs.
285 Through prospectively sequencing Actinomycetes using Flongle, it was empirically evaluated in the
286 current study.

287 An interesting observation on BGC analysis was that active site specificity for various BGC classes (NRPS,
288 PKS and CDPS) in the Flongle assemblies were correctly predicted. The active site specificities were used
289 by PRISM to generate possible structures, which were then used to query MS/MS data for potential
290 spectral matches. A spectrum match to a predicted structure indirectly proves that active site
291 specificities were correct, for instance, in the case of cWW. However, we also observed that frameshifts
292 and sequencing errors affected in silico prediction of accurate structures for some BGCs.

293 The analysis of RiPP BGCs in flongle assemblies was relatively less affected by sequencing. RiPP
294 metabolite prediction is based on short precursor peptide and BGC prediction relies on detecting post-
295 translational modifying enzymes through error-tolerant profile Hidden Markov models. The chance of a
296 mismatch underlying a 100 nucleotide (30-mer core peptide sequence) is low. For example, 19,227
297 mismatches were detected in total in a flongle assembly relative to PacBio, which corresponds to a
298 chance of less than one mismatch per 100 nt ($19,227 \text{ mismatches} / 7183038 \text{ nt genome size} \times 100 \text{ nt} =$
299 $0.26 \text{ per } 100 \text{ nt}$). This is evident through accurate prediction of a new lassopeptide BGC and its
300 corresponding experimental mass spectrum in the extract from strain GA6-002.

301 Similarly, BGCs homologous to previously characterized BGCs for known metabolites can be identified
302 through sequence similarity searches. The consensus accuracy of the assemblies was observed to be
303 99.5% accurate, which makes a genome sequence suitable for comparison with known BGC sequences

304 or to compute average nucleotide identify with published genomes. We demonstrated this through the
305 rediscovery of BGCs and selected Actinomycetes siderophores.

306 While our results suggest Flongle is a useful platform for sequencing Actinomycetes, increased
307 consistency in total sequencing output might enable further optimized workflows. For instance, Flongle
308 flow cells were less consistent in the number of starting pores (<60 out of an expected 126 in most
309 cases), which affected total sequencing output and lower than desired coverage for a few samples. A
310 consistent and anticipated number of pores (>100) across experiments would allow for higher
311 sequencing coverage using the same experimental workflow or allow more genomes to be sequenced in
312 an experiment.

313 While a few BGCs could be connected to the metabolites in the current study, most remained
314 unconnected. Connecting BGCs to metabolites is a multi-factor problem not limited by sequencing
315 accuracy alone. Improvements in experiments and computational algorithms would be needed to
316 circumvent this issue in the future. First, it is highly unlikely that all BGCs will be expressed when strains
317 are grown in only two culture media as tested here; thus, additional media and growth conditions or
318 genetics-free elicitor screens should be used (26-28). Second, only PRISM in silico predicted structures
319 were used. In the future, a more extensive in silico structure generation that addresses ambiguous
320 active site specificities (e.g., two or more possible amino acids at a site in NRPS) could be used. Third,
321 MS/MS data were queried for exact compound spectral matches. Minor differences between predicted
322 and expressed metabolites (e.g., single-site methylation or hydroxylation) would result in a mass shift,
323 and a match would not be possible.

324 In summary, multiplexed low coverage sequencing of Actinomycetes genomes on Flongle is a promising
325 option for the genome-guided discovery of natural products. Numerous research laboratories house
326 valuable bacterial strain collections (29-34). Limited by the costs of large-scale long read sequencing,
327 genome sequencing of natural product producing bacteria usually occurs on a strain-by-strain basis
328 {Sun, 2021 #295;Li, 2021 #316;Yang, 2021 #317;Braesel, 2018 #326}. The future of natural product
329 research is expected to involve analysis of genomics and metabolomics data using genome mining (e.g.
330 antiSMASH and PRISM) and mass spectrum matching tools (such as molDiscovery integrated with
331 NPAtlas-like databases used in this study). Indeed, such efforts are already taking place on metagenomic
332 data sets (38, 39); while those studies provide vast amounts of data on the natural products-ome, a key
333 limitation is that the data are not connected to archived bacterial strains. It is our hope that low-cost
334 sequencing workflows such as the one described here may allow for access to genome sequencing on a
335 larger scale and/or to a broader community of researchers, especially in resource-limited settings.

336

337 Materials and Methods

338

339 Strain isolation

340 The twenty sequenced strains were a subset of streptomycin, novobiocin or vancomycin resistant strains
341 from an in-house Actinomycetes strain library housed in the Laboratory of Bioorganic Chemistry,
342 National Institutes of Health. The strains were isolated from soil specimens collected from deserts in
343 Arizona, California and Nevada through standard procedures described in a previous study (35).

344 Nanopore sequencing

345 Each strain was cultivated for 3-7 days in 10 mL of Tryptic Soy broth (BD Diagnostic, catalog no. 211768)
346 with 0.5% (w/v) glycine from frozen glycerol stocks. The cultures were centrifuged at 10,000 x g for 10
347 minutes and cell pellets were resuspended into 250 μ L Tris EDTA (TE) buffer followed by addition of 50
348 μ L of lysosome (100 mg/ml). The mixture was incubated overnight (16 hrs) at 37° C. The next morning
349 10 μ L of RNase A (10 mg/ μ L) was added to the cell lysate and incubated for an additional 20 min after
350 which 250 μ L of proteinase K (400 μ g/ μ L) was added and incubated for 2 hours. DNA was purified from
351 cell lysates using 1:1 v/v phenol-chloroform extraction and the DNA was collected from the upper phase.
352 Genomic DNA was precipitated with 0.7 volume of isopropanol, washed with 80% ethanol, and
353 resuspended into 50 μ L TE.

354 DNA libraries were prepared using Oxford Nanopore Ligation Sequencing Kit (SQK-LSK109) and the
355 native barcoding kit (NBD104) protocol for Flongle with some modifications. A DNA fragmentation step
356 was not performed. 500 ng of genomic DNA was directly processed for DNA end repair with NEBNext
357 Ultra II End repair/dA-tailing Module (New England Biolabs, catalog no. E7546). Barcodes were ligated to
358 the end-repaired DNA and purified with 0.1x or 0.15x beads (Omega Bio-Tek Inc, catalog no. M1378-01),
359 resuspended in a custom buffer (10 mM Tris-Cl pH 8.0, 1 mM EDTA, 0.5 M MgCl₂ and 5% PEG). A pooled
360 library was prepared by combining 62.5 ng of each barcoded DNA. Nanopore adapters were ligated to
361 the pooled library followed by library loading and sequencing according to the manufacturer's
362 instructions.

363 Data-dependent untargeted LC-MS/MS

364 Each strain was cultivated in deep well plates containing 400 μ L of ISP1 (BD Diagnostic, catalog no
365 276910) or R2A media (Teknova, catalog no. R0005). The cultures were incubated at 30° C with shaking
366 at 200 rpm for one week before extraction with an equal volume of ethyl acetate followed by extraction
367 with *n*-butanol. Uninoculated media were used as blanks / negative control, and any metabolite
368 observed in a blank run was excluded from interpretation. The LC-MS/MS data was collected using an
369 Agilent 1290 Infinity II UPLC system equipped with an Agilent 6545 qTOF mass spectrometer. Samples
370 were chromatographed on a Agilent Eclipse Plus C18 2.1x50mm column (3 μ L injections) using a
371 gradient of 99% A (0.1% formic acid in water) to 95% B (acetonitrile) at a flow rate of 0.5mL/min over
372 10min. MS/MS fragmentation was carried out in auto mode with collision energies of 10, 20 and 40 KeV
373 excluding precursor ions in the range of 40-180 *m/z* and abundance below 7,000 counts.

374 Data analysis

375

376 Genomics

377 Primary genomic data analysis was conducted by basecalling with guppy (version 4.2.2, model
378 dna_r9.4.1_450bps_hac.cfg), demultiplexing with Qcat (version 1.0.6) and assembling with Canu
379 (version 2.0) (40). Canu assemblies were constructed with an expected genome size of 8 Mb, minimum
380 read length threshold of 1 Kb, minimum coverage of 2, and high Mhap error correction sensitivity (40).
381 The genome assemblies were polished by aligning reads to the assembly and calling consensus with
382 Racon and Medeka (41). Genes and secondary metabolite gene clusters were predicted using the
383 programs antiSMASH (version 5) and PRISM (version 4.4.5) (11).

384 [Assessing effect of sequencing coverage on BGC detection](#)

385 FastQ reads for previously sequenced Actinomycete genomes were downloaded from the European
386 Nucleotide Archive, downsampled to an estimated coverage of 60x, 30x, 15x and 7x using seqtk
387 (assuming an 8 Mb genome as in prospective sequencing) (Table S 1). Seqtk allows random subsampling
388 of reads. Reads were subsampled to desired coverage according to the following estimation: number of
389 reads for Q coverage = $(Q/\text{original coverage}) \times \text{original number of reads}$. The downsampled FastQ files
390 were assembled with Canu, polished with Medeka and BGCs predicted using antiSMASH. The number of
391 mismatches in each assembly relative to original coverage was calculated using Quast (42). For
392 consistency with data from this study (presented in Figure 3), the coverage presented is aligned
393 coverage, taking into account the size of the final assembly and not the expected size (i.e. 8 Mb). The
394 mapped coverage was extracted from Canu assembler tig information files.

395 [BGC comparison between strains](#)

396 The antiSMASH-predicted BGC sequences were extracted from each strain's genome assemblies and
397 aligned in all possible strain pair combinations using minimap2, allowing for 5% sequence divergence
398 (43). If a BGC from strain-1 did not align to any of the BGCs in strain-2, it was considered absent in
399 strain-2.

400 [Homologous BGCs of previously characterized metabolites](#)

401 Homologous BGCs of previously characterized metabolites were obtained through the 'known cluster
402 blast' module of antiSMASH. The output of the program contains gene-wise blast hits for each BGC in
403 the genome to BGCs in MiBiG (4). To identify the best hit in MiBiG database, output was first filtered to
404 obtain MiBiG BGCs that share the largest number of genes, highest mean percent identity and highest
405 mean coverage with genes in the query BGC. The results were subsequently filtered to retain only BGCs
406 where the ratio of lengths between query and MiBiG BGCs was between 0.7 to 1.1.

407 [LC MS/MS Analysis](#)

408 Analysis of LC MS/MS data was conducted by conversion of the vendor.d format to mzXML files using
409 the GNPS conversion utility. These mzXML files were subsequently used for all analyses.

410 [Spectrum matching - known or unknown structures](#)

411 Spectrum matches for known metabolites using the Natural Product Atlas or unknown metabolites
412 (PRISM predicted structures) were identified by using molDiscovery (3, 12). molDiscovery computes
413 theoretical MS/MS spectra of compounds in the database, identifies spectrum matches at user-defined
414 mass-tolerance, and subsequently calculates statistical significance by matching the spectrum against a
415 decoy database. In this analysis, mass tolerance of 20 ppm, p-value less than e^{-10} and FDR less than 1%
416 were considered.

417 RiPPs

418 Spectrum matches for RiPPs were detected using metaminer (14). Given a list of short peptides,
419 metaminer constructs possible RiPP products based on knowledge of post-translational modifications
420 within RiPPs. It then predicts an MS/MS spectrum for each predicted RiPP product and conducts a
421 search of experimentally collected MS/MS spectra for potential matches. All open-reading-frames
422 (ORFs) shorter than 600 nt (200 amino acids) located within RiPP BGCs predicted by antiSMASH or
423 PRISM were used for this analysis.

424 Integration of the mass spectrometry and genomic sequences was achieved through R scripts and
425 several packages including MSnbase (44) and Open Babel (45).

426 Data availability

427 Raw sequencing data are available under NCBI Project accession no: PRJNA752621. Genome assemblies
428 and additional data are available at Figshare (https://figshare.com/articles/dataset/_/15094044). The
429 MS/MS spectra have been uploaded to GNPS with accession number: MSV000087950. Scripts used in
430 data analysis and preparation of figures are available at
431 https://github.com/rajwanir/flongle_actinomycetes_paper .

432

433 Acknowledgements

434 This work was supported by the NIH Intramural Research Program (NIDDK) and utilized the
435 computational resources of the NIH HPC Biowulf cluster (<http://hpc.nih.gov>).

Figures

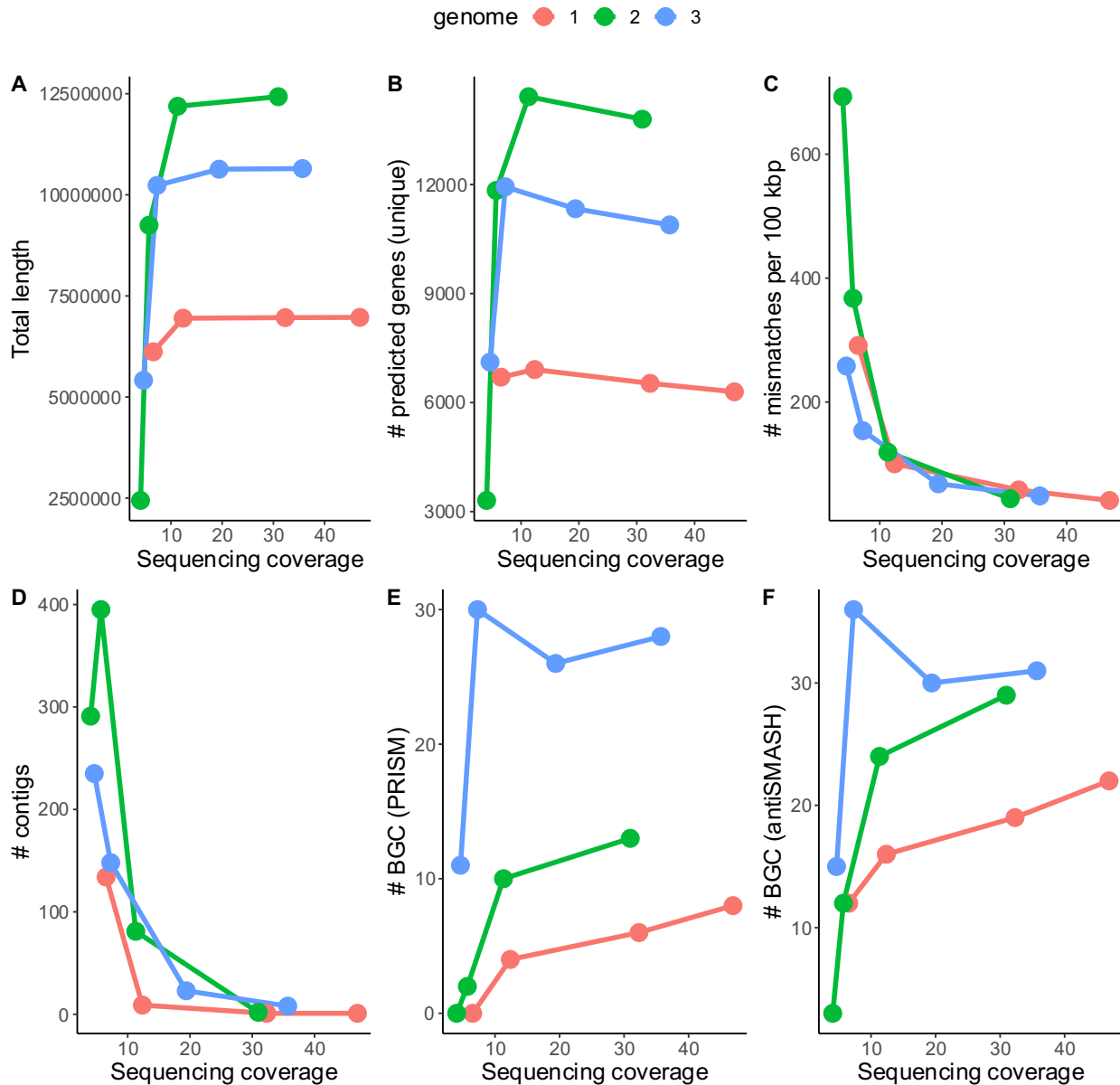


Figure 1: An in silico analysis of the effect of sequencing coverage on assembly quality and BGC prediction.

Three genomes previously sequenced at high coverage on ONT MinION/GridION platform were down sampled to the indicated sequencing coverages and then assembled. A-F The quality of the assembly as indicated by total assembly length, number of contigs, number of mismatches per 100 Kb and number of unique predicted genes are shown along with the number of BGCs predicted by antiSmash. The sequencing data for this analysis was downloaded from the European Nucleotide Archive. Accession numbers: 1 = SRR10597857, 2 = SRR9710049, 3 = DRR240480).

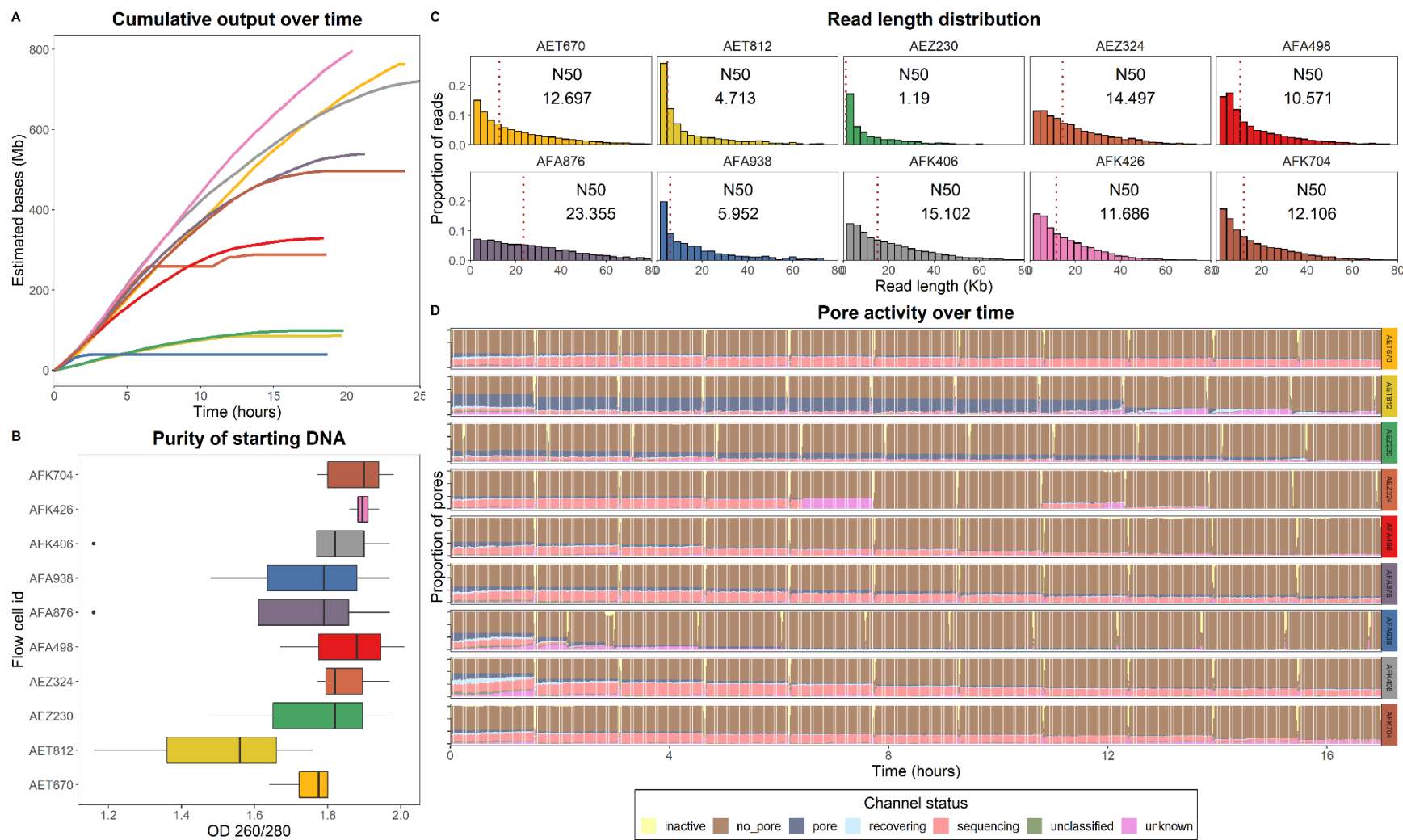


Figure 2: Library preparation and sequencing quality metrics.

The data in each panel (A-D) are colored and grouped by flow cell as indicated in panel B. Panel A indicates cumulative output (estimated megabases) over time (hours) across 10 sequencing experiments. Panel B indicates the purity (nanodrop 260/280 ratio) for samples run in each experiment. Panel C indicates read length distribution across experiments. Read N50 value (50% of bases are

in reads longer this value) in each experiment is labeled. Panel D shows run performance at the pore level in each experiment except AFK4226. The AFK4226 experiment was interrupted at the end and the instrument did not generate the pore activity metadata to include in this chart. “Sequencing” indicates that the pore is occupied with DNA and is sequencing. “Pore” indicates an empty pore with no DNA, “no pore” indicates an inactive pore (i.e. unavailable for sequencing).

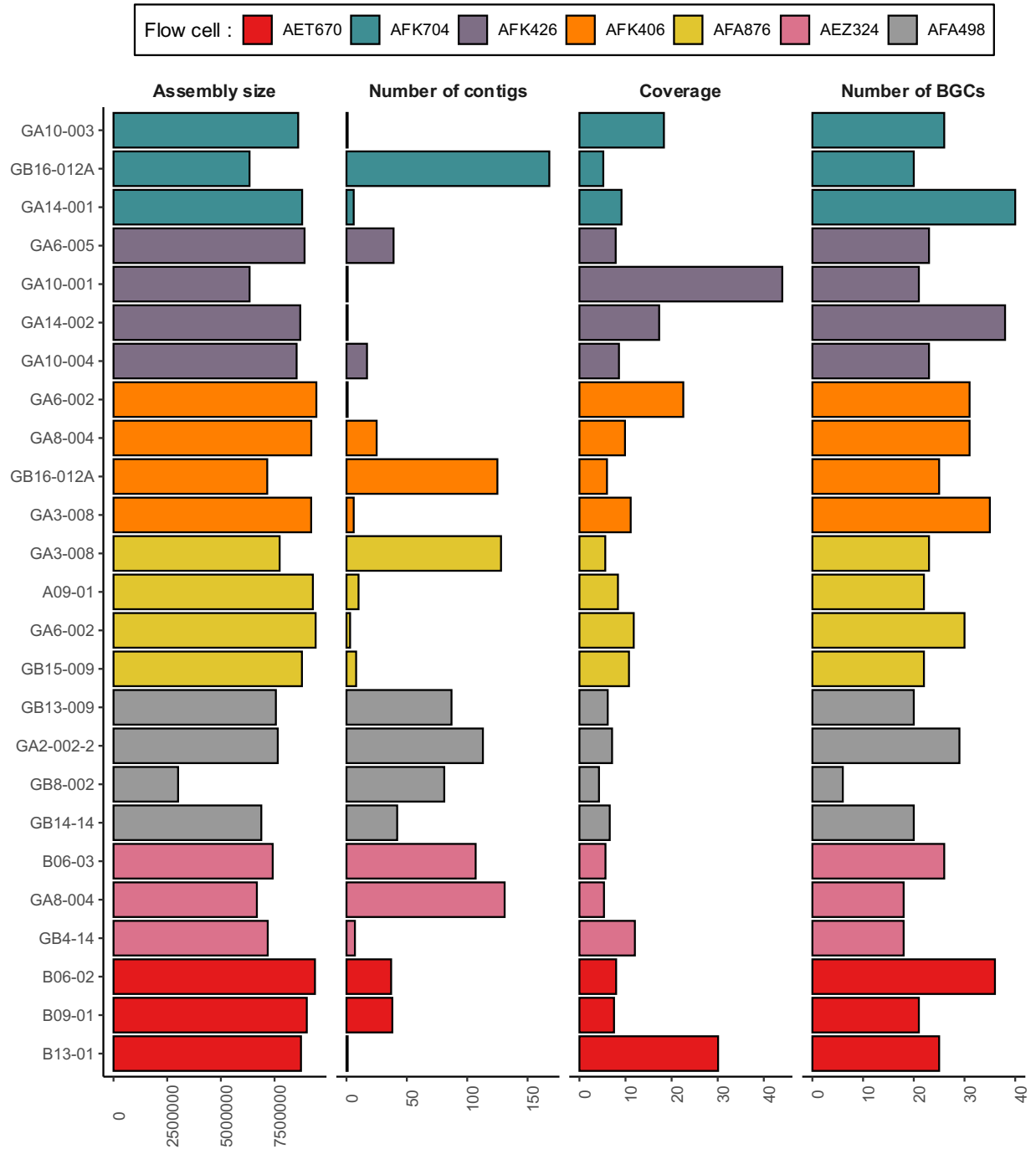


Figure 3: Characteristics of the genome assemblies obtained through low-pass multiplexed sequencing on Flongle. Each bar represents a sample. Bars are grouped and colored by flow cells (individual sequencing experiment).

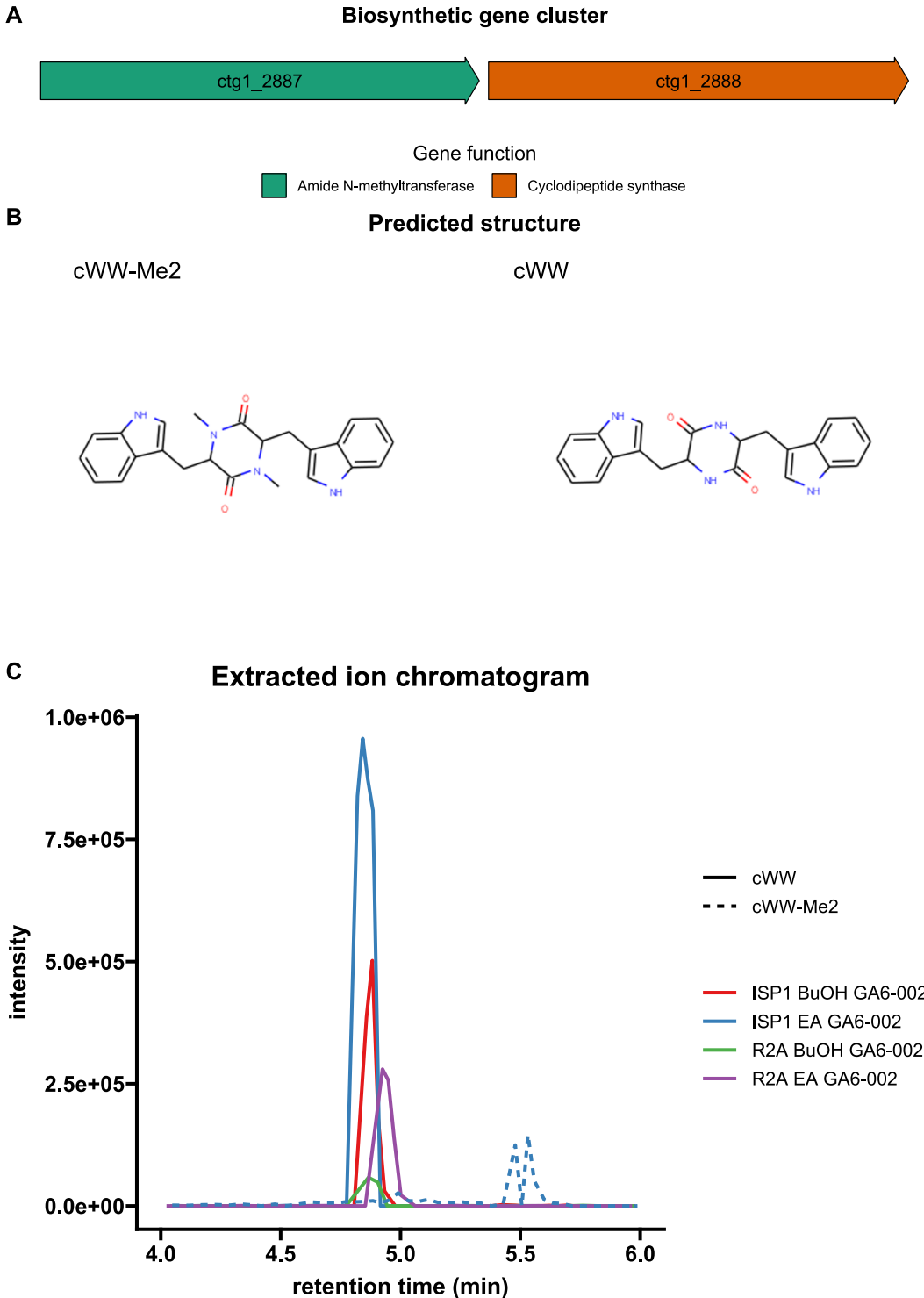


Figure 4: An *N*-methylated cyclo(Trp-Trp) cyclic dipeptide detected in *Amycolatopsis* sp. GA6-002 and its corresponding BGC. A) Cyclic dipeptide BGC and B) the structures predicted by PRISM based on predicted specificity of the cyclic dipeptide synthase. C) Extracted ion chromatogram for cyclic di tryptophan (cWW) and its *N*-methylated derivative (cWW-Me2) observed in four separate crude extracts.

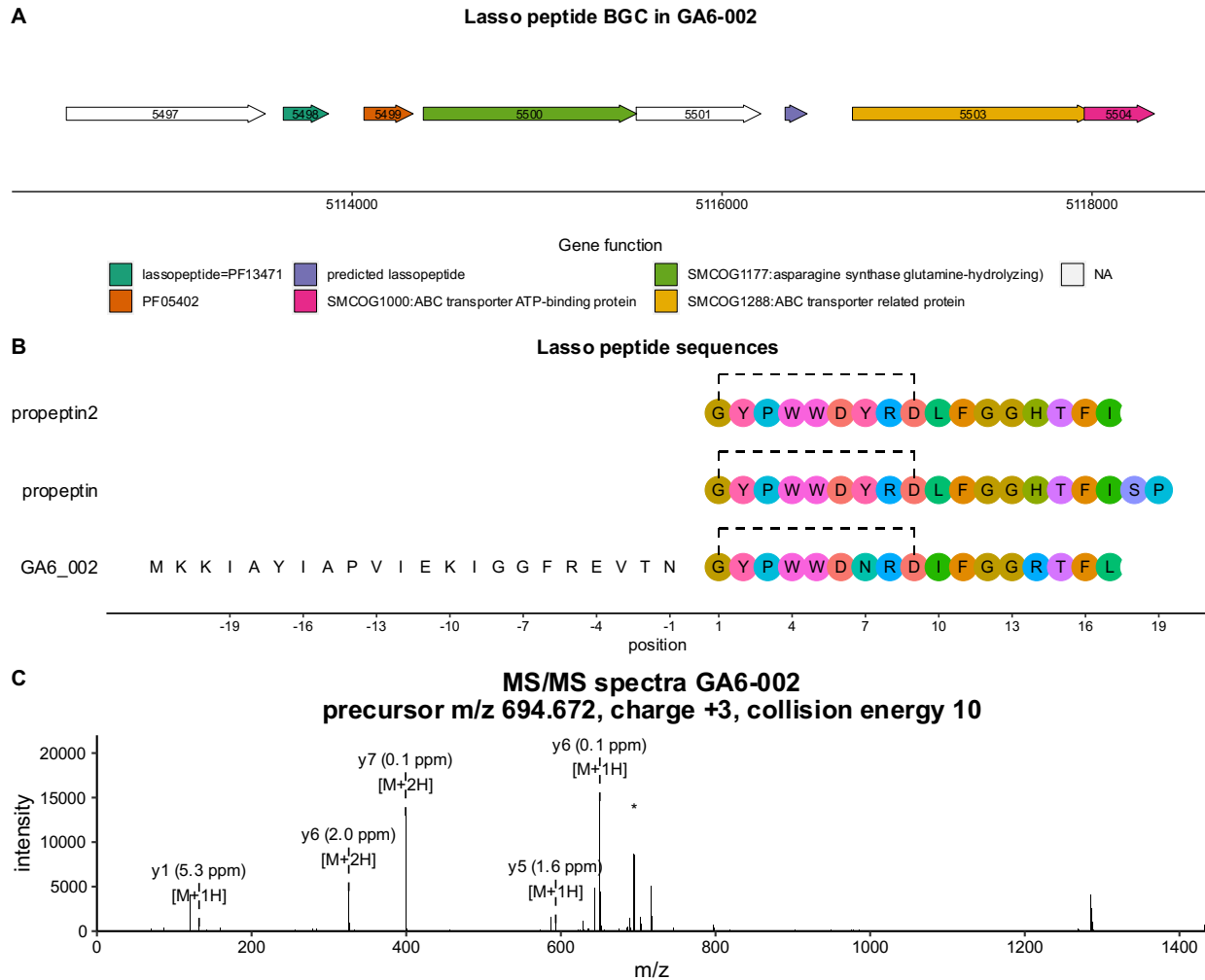


Figure 5: A new lasso peptide variant identified in GA6-002.

A) Lasso peptide biosynthetic gene cluster. Genes are colored according to their functions. B) Lasso peptide sequences in propeptin2, propeptin and GA6-002 (this study). Amino acid positions for leader sequence are shown as negative numbers. A BGC for propeptin 2 and propeptin has yet to be characterized and therefore the leader sequences are not shown for them. Dashed line between Gly and Asp shows the position of crosslink. C) MS/MS spectra that matches to the post-translationally modified predicted core sequence in GA6-002.

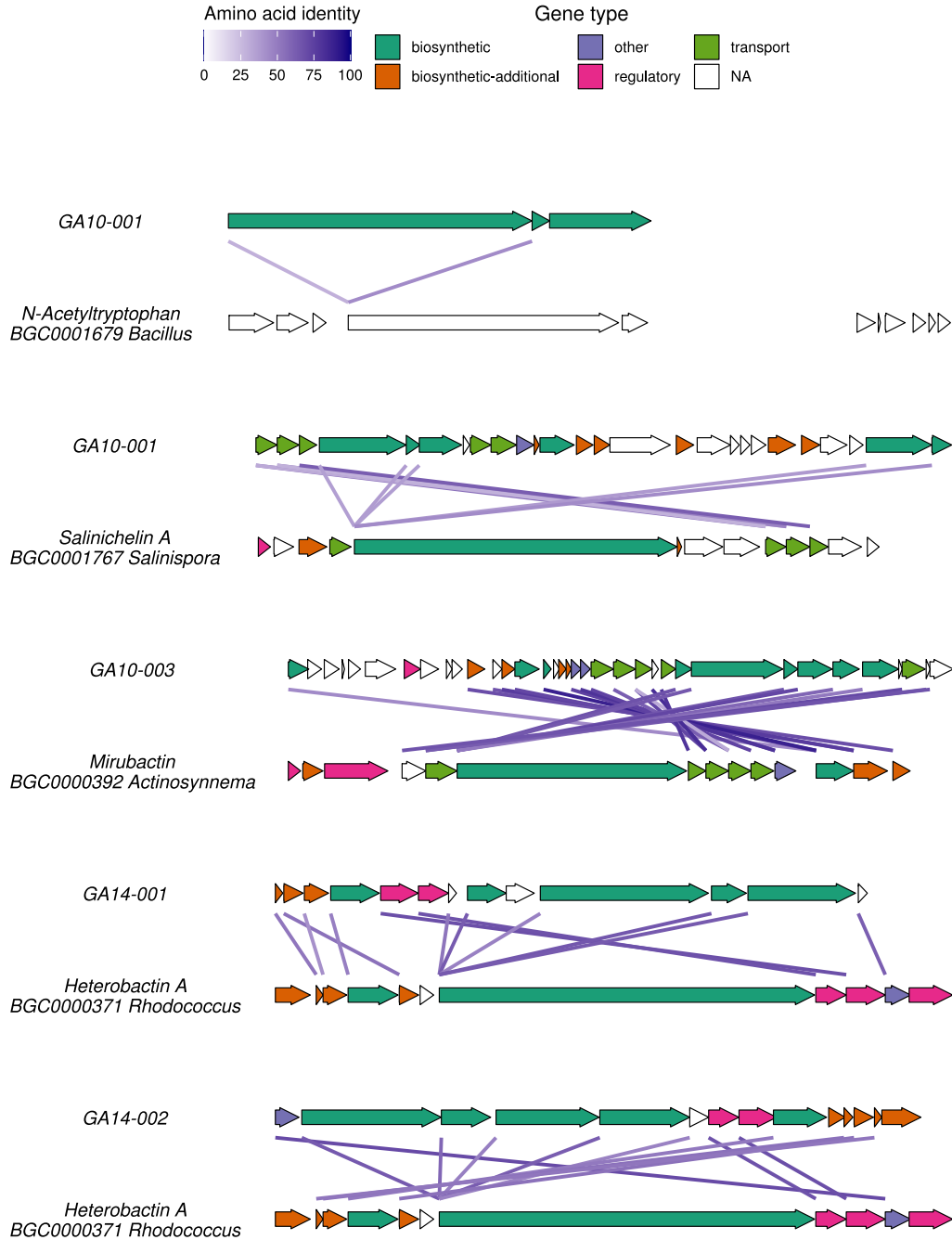


Figure 6: Homologous BGCs mapped for known metabolites detected in LC-MS/MS.

Alignments of BGCs in the MiBiG database to those identified in a producing strain from this study. Genes are colored according to function. Lines between genes indicate similarity between genes with its color intensity proportional to the BLAST amino acid identity.

Tables

Table 1: Quality assessment of genomes of two strains (GA3-008 and GB4-14) obtained from low coverage flongle assemblies, compared to PacBio and MinION assemblies.

Attribute	GA3-008		GB4-14	
	Flongle multiplex	Minion singleplex	Flongle multiplex	PacBio
Est. coverage	15.3	121.65	14	200
# contigs	6	1	7	2
Assembly size	9205503	9199325	7183038	7163416
# mismatches*	3000	-	19227	-
# indels *	13803	-	14484	-
# BGCs	35	40	18	18

*Number of mismatches and indels in the Flongle multiplexed assemblies are relative to the same strain sequenced by either MinION or PacBio.

References

1. Organization WH. 2019. No time to wait: Securing the future from drug-resistant infections. *World Health Organization: Geneva, Switzerland*.
2. Genilloud O. 2017. Actinomycetes: still a source of novel antibiotics. *Nat Prod Rep* 34:1203-1232.
3. van Santen JA, Jacob G, Singh AL, Aniebok V, Balunas MJ, Bunsko D, Neto FC, Castaño-Espriu L, Chang C, Clark TN, Cleary Little JL, Delgadillo DA, Dorrestein PC, Duncan KR, Egan JM, Galey MM, Haeckl FPJ, Hua A, Hughes AH, Iskakova D, Khadilkar A, Lee J-H, Lee S, LeGrow N, Liu DY, Macho JM, McCaughey CS, Medema MH, Neupane RP, O'Donnell TJ, Paula JS, Sanchez LM, Shaikh AF, Soldatou S, Terlouw BR, Tran TA, Valentine M, van der Hooft JJJ, Vo DA, Wang M, Wilson D, Zink KE, Linington RG. 2019. The Natural Products Atlas: an open access knowledge base for microbial natural products discovery. *ACS Cent Sci* 5:1824-1833.
4. Kautsar SA, Blin K, Shaw S, Navarro-Muñoz JC, Terlouw BR, van der Hooft JJJ, van Santen JA, Tracanna V, Suarez Duran HG, Pascal Andreu V, Selem-Mojica N, Alanjary M, Robinson SL, Lund G, Epstein SC, Sisto AC, Charkoudian LK, Collemare J, Linington RG, Weber T, Medema MH. 2019. Mibig 2.0: A repository for biosynthetic gene clusters of known function. *Nucl Acids Res* 48:D454-D458.
5. Navarro-Muñoz JC, Selem-Mojica N, Mullowney MW, Kautsar SA, Tryon JH, Parkinson EI, De Los Santos ELC, Yeong M, Cruz-Morales P, Abubucker S, Roeters A, Lokhorst W, Fernandez-Guerra A, Cappelini LTD, Goering AW, Thomson RJ, Metcalf WW, Kelleher NL, Barona-Gomez F, Medema MH. 2020. A computational framework to explore large-scale biosynthetic diversity. *Nat Chem Biol* 16:60-68.
6. Kloosterman AM, Cimermanic P, Elsayed SS, Du C, Hadjithomas M, Donia MS, Fischbach MA, van Wezel GP, Medema MH. 2020. Expansion of RiPP biosynthetic space through integration of pan-genomics and machine learning uncovers a novel class of lantibiotics. *PLoS Biol* 18:e3001026.
7. Ganley JG, Pandey A, Sylvester K, Lu K-Y, Toro-Moreno M, Rütchlin S, Bradford JM, Champion CJ, Böttcher T, Xu J, Derbyshire ER. 2020. A systematic analysis of mosquito-microbiome biosynthetic gene clusters reveals antimalarial siderophores that reduce mosquito reproduction capacity. *Cell Chem Biol* 27:817-826.
8. Medema MH, Blin K, Cimermanic P, de Jager V, Zakrzewski P, Fischbach MA, Weber T, Takano E, Breitling R. 2011. Antismash: Rapid identification, annotation and analysis of secondary metabolite biosynthesis gene clusters in bacterial and fungal genome sequences. *Nucl Acids Res* 39:W339-W346.
9. Meleshko D, Mohimani H, Tracanna V, Hajirasouliha I, Medema MH, Korobeynikov A, Pevzner PA. 2019. Biosyntheticspades: Reconstructing biosynthetic gene clusters from assembly graphs. *Genome Res* 29:1352-1362.
10. Stortchevoi A, Kamelamela N, Levine SS. 2020. SPRI beads-based size selection in the range of 2-10 kb. *J Biomol Tech* doi:10.7171/jbt.20-3101-002:jbt.20-3101-3002.
11. Skinnider MA, Johnston CW, Gunabalasingam M, Merwin NJ, Kieliszek AM, MacLellan RJ, Li H, Ranieri MRM, Webster ALH, Cao MPT, Pfeifle A, Spencer N, To QH, Wallace DP, Dejong CA, Magarvey NA. 2020. Comprehensive prediction of secondary metabolite structure and biological activity from microbial genome sequences. *Nature Commun* 11:6058.
12. Hosein M, Liu C, Mustafa G, Azat T, Alexey G. 2021. MolDiscovery: Learning mass spectrometry fragmentation of small molecules. *Nature Comm* doi:10.21203/rs.3.rs-71854/v1.
13. Giessen TW, von Tesmar AM, Marahiel MA. 2013. A trna-dependent two-enzyme pathway for the generation of singly and doubly methylated ditryptophan 2,5-diketopiperazines. *Biochemistry* 52:4274-4283.

14. Cao L, Gurevich A, Alexander KL, Naman CB, Leão T, Glukhov E, Luzzatto-Knaan T, Vargas F, Quinn R, Bouslimani A, Nothias LF, Singh NK, Sanders JG, Benitez RAS, Thompson LR, Hamid M-N, Morton JT, Mikheenko A, Shlemov A, Korobeynikov A, Friedberg I, Knight R, Venkateswaran K, Gerwick WH, Gerwick L, Dorrestein PC, Pevzner PA, Mohimani H. 2019. MetaMiner: A scalable peptidogenomics approach for discovery of ribosomal peptide natural products with blind modifications from microbial communities. *Cell Systems* 9:600-608.e604.
15. Tietz JI, Schwalen CJ, Patel PS, Maxson T, Blair PM, Tai H-C, Zakai UI, Mitchell DA. 2017. A new genome-mining tool redefines the lasso peptide biosynthetic landscape. *Nat Chem Biol* 13:470-478.
16. Meteleev M, Tietz JI, Melby JO, Blair PM, Zhu L, Livnat I, Severinov K, Mitchell DA. 2015. Structure, bioactivity, and resistance mechanism of streptomonicin, an unusual lasso peptide from an understudied halophilic actinomycete. *Chem Biol* 22:241-250.
17. Kimura K, Kanou F, Takahashi H, Esumi Y, Uramoto M, Yoshihama M. 1997. Propeptin, a new inhibitor of prolyl endopeptidase produced by microbispora. I. Fermentation, isolation and biological properties. *J Antibiot (Tokyo)* 50:373-378.
18. Choi WS, Wu X, Choeng YH, Mahmud T, Jeong BC, Lee SH, Chang YK, Kim CJ, Hong SK. 2008. Genetic organization of the putative salbostatin biosynthetic gene cluster including the 2-epi-5-epi-valiolone synthase gene in *Streptomyces albus* atcc 21838. *Appl Microbiol Biotechnol* 80:637-645.
19. Schlorke O, Krastel P, Muller I, Uson I, Dettner K, Zeek A. 2002. Structure and biosynthesis of cetoniacytone a, a cytotoxic aminocarba sugar produced by an endosymbiotic actinomycetes. *J Antibiot (Tokyo)* 55:635-642.
20. Wu X, Flatt PM, Xu H, Mahmud T. 2009. Biosynthetic gene cluster of cetoniacytone a, an unusual aminocyclitol from the endosymbiotic bacterium actinomycetes sp. Lu 9419. *Chembiochem* 10:304-314.
21. Heide L. 2009. The aminocoumarins: Biosynthesis and biology. *Nat Prod Rep* 26:1241-1250.
22. Kim CG, Lamichhane J, Song KI, Nguyen VD, Kim DH, Jeong TS, Kang SH, Kim KW, Maharjan J, Hong YS, Kang JS, Yoo JC, Lee JJ, Oh TJ, Liou K, Sohng JK. 2008. Biosynthesis of rubradirin as an ansamycin antibiotic from *Streptomyces achromogenes* var. *Rubradiris nrrl3061*. *Arch Microbiol* 189:463-473.
23. Castro JF, Razmilic V, Gomez-Escribano JP, Andrews B, Asenjo JA, Bibb MJ. 2015. Identification and heterologous expression of the chaxamycin biosynthesis gene cluster from *Streptomyces leeuwenhoekii*. *App Environ Microbiol* 81:5820.
24. Truman AW, Kwun MJ, Cheng J, Yang SH, Suh J-W, Hong H-J. 2014. Antibiotic resistance mechanisms inform discovery: Identification and characterization of a novel *Amycolatopsis* strain producing ristocetin. *Antimicrob Agents Chemother* 58:5687-5695.
25. Culp EJ, Waglechner N, Wang W, Fiebig-Comyn AA, Hsu YP, Koteva K, Sychantha D, Coombes BK, Van Nieuwenhze MS, Brun YV, Wright GD. 2020. Evolution-guided discovery of antibiotics that inhibit peptidoglycan remodelling. *Nature* 578:582-587.
26. Bode HB, Bethe B, Hofs R, Zeek A. 2002. Big effects from small changes: Possible ways to explore nature's chemical diversity. *Chembiochem* 3:619-627.
27. Liu M, Grkovic T, Liu X, Han J, Zhang L, Quinn RJ. 2017. A systems approach using OSMAC, log p and NMR fingerprinting: An approach to novelty. *Synth Syst Biotechnol* 2:276-286.
28. Xu F, Wu Y, Zhang C, Davis KM, Moon K, Bushin LB, Seyedsayamdost MR. 2019. A genetics-free method for high-throughput discovery of cryptic microbial metabolites. *Nat Chem Biol* 15:161-168.
29. Amiri Moghaddam J, Crusemann M, Alanjary M, Harms H, Davila-Céspedes A, Blom J, Poehlein A, Ziemert N, König GM, Schaberle TF. 2018. Analysis of the genome and metabolome of marine myxobacteria reveals high potential for biosynthesis of novel specialized metabolites. *Sci Rep* 8:16600.
30. Bader CD, Panter F, Muller R. 2020. In depth natural product discovery - myxobacterial strains that provided multiple secondary metabolites. *Biotechnol Adv* 39:107480.

31. Hernandez A, Nguyen LT, Dhakal R, Murphy BT. 2021. The need to innovate sample collection and library generation in microbial drug discovery: A focus on academia. *Nat Prod Rep* 38:292-300.
32. Jensen PR, Moore BS, Fenical W. 2015. The marine actinomycete genus *Salinispora*: A model organism for secondary metabolite discovery. *Nat Prod Rep* 32:738-751.
33. Steele AD, Teijaro CN, Yang D, Shen B. 2019. Leveraging a large microbial strain collection for natural product discovery. *J Biol Chem* 294:16567-16576.
34. Waglechner N, McArthur AG, Wright GD. 2019. Phylogenetic reconciliation reveals the natural history of glycopeptide antibiotic biosynthesis and resistance. *Nat Microbiol* 4:1862-1871.
35. Sun J, Zhao G, O'Connor RD, Davison JR, Bewley CA. 2021. Vertirhodins A–F, C-linked pyrrolidine-aminosugar-containing pyranonaphthoquinones from *Streptomyces* sp. B15-008. *Org Lett* 23:682-686.
36. Li H, Zhang M, Li H, Yu H, Chen S, Wu W, Sun P. 2021. Discovery of venturicin congeners and identification of the biosynthetic gene cluster from *Streptomyces* sp. Nrrl s-4. *J Nat Prod* 84:110-119.
37. Yang J, Song Y, Tang M-C, Li M, Deng J, Wong N-K, Ju J. 2021. Genome-directed discovery of tetrahydroisoquinolines from deep-sea derived *Streptomyces niveus* SCSIO 3406. *J Org Chem* doi:10.1021/acs.joc.1c00123.
38. Sharrar AM, Crits-Christoph A, Méheust R, Diamond S, Starr EP, Banfield JF. 2020. Bacterial secondary metabolite biosynthetic potential in soil varies with phylum, depth, and vegetation type. *Mbio* 11:e00416-00420.
39. Nayfach S, Roux S, Seshadri R, Udway D, Varghese N, Schulz F, Wu D, Paez-Espino D, Chen IM, Huntemann M, Palaniappan K, Ladau J, Mukherjee S, Reddy TBK, Nielsen T, Kirton E, Faria JP, Edirisinghe JN, Henry CS, Jungbluth SP, Chivian D, Dehal P, Wood-Charlson EM, Arkin AP, Tringe SG, Visel A, Abreu H, Acinas SG, Allen E, Allen MA, Andersen G, Anesio AM, Attwood G, Avila-Magaña V, Badis Y, Bailey J, Baker B, Baldrian P, Barton HA, Beck DAC, Becraft ED, Beller HR, Beman JM, Bernier-Latmani R, Berry TD, Bertagnolli A, Bertilsson S, Bhatnagar JM, Bird JT, Blumer-Schuette SE, Bohannon B, Borton MA, Brady A, Brawley SH, Brodie J, Brown S, Brum JR, Brune A, Bryant DA, Buchan A, Buckley DH, Buongiorno J, Cadillo-Quiroz H, Caffrey SM, Campbell AN, Campbell B, Carr S, Carroll J, Cary SC, Cates AM, Cattolico RA, Cavicchioli R, Chistoserdova L, Coleman ML, Constant P, Conway JM, Mac Cormack WP, Crowe S, Crump B, Currie C, Daly R, Denef V, Denman SE, Desta A, Dionisi H, Dodsworth J, Dombrowski N, Donohue T, Dopson M, Driscoll T, Dunfield P, Dupont CL, Dynarski KA, Edgcomb V, Edwards EA, Elshahed MS, Figueroa I, Flood B, Fortney N, Fortunato CS, Francis C, Gachon CMM, Garcia SL, Gazitua MC, Gentry T, Gerwick L, Gharechahi J, Girguis P, Gladden J, Gradoville M, Grasby SE, Gravuer K, Grettenberger CL, Gruninger RJ, Guo J, Habteselassie MY, Hallam SJ, Hatzenpichler R, Hausmann B, Hazen TC, Hedlund B, Henny C, Herfort L, Hernandez M, Hershey OS, Hess M, Hollister EB, Hug LA, Hunt D, Jansson J, Jarett J, Kadnikov VV, Kelly C, Kelly R, Kelly W, Kerfeld CA, Kimbrel J, Klassen JL, Konstantinidis KT, Lee LL, Li W-J, Loder AJ, Loy A, Lozada M, MacGregor B, Magnabosco C, Maria da Silva A, McKay RM, McMahan K, McSweeney CS, Medina M, Meredith L, Mizzi J, Mock T, Momper L, Moran MA, Morgan-Lang C, Moser D, Muyzer G, Myrold D, Nash M, Nesbø CL, Neumann AP, Neumann RB, Noguera D, Northen T, Norton J, Nowinski B, Nüsslein K, O'Malley MA, Oliveira RS, Maia de Oliveira V, Onstott T, Osvatic J, Ouyang Y, Pachiadaki M, Parnell J, Partida-Martinez LP, Peay KG, Pelletier D, Peng X, Pester M, Pett-Ridge J, Peura S, Pjevac P, Plominsky AM, Poehlein A, Pope PB, Ravin N, Redmond MC, Reiss R, Rich V, Rinke C, Rodrigues JLM, Rossmassler K, Sackett J, Salekdeh GH, Saleska S, Scarborough M, Schachtman D, Schadt CW, Schrenk M, Sczyrba A, Sengupta A, Setubal JC, Shade A, Sharp C, Sherman DH, Shubenkova OV, Sierra-Garcia IN, Simister R, Simon H, Sjöling S, Slonczewski J, Correa de Souza RS, Spear JR, Stegen JC, Stepanauskas R, Stewart F, Suen G, Sullivan M, Sumner D, Swan BK, Swingley W, Tarn J, Taylor GT, Teeling H, Tekere M, Teske A, Thomas T, Thrash C, Tiedje J, Ting CS, Tully B,

- Tyson G, Ulloa O, Valentine DL, Van Goethem MW, VanderGheynst J, Verbeke TJ, Vollmers J, Vuillemin A, Waldo NB, Walsh DA, Weimer BC, Whitman T, van der Wielen P, Wilkins M, Williams TJ, Woodcroft B, Woolet J, Wrighton K, Ye J, Young EB, Youssef NH, Yu FB, Zenskaya TI, Ziels R, Woyke T, Mouncey NJ, Ivanova NN, Kyrpides NC, Elie-Fadrosh EA, Consortium IMD. 2020. A genomic catalog of earth's microbiomes. *Nature Biotech* doi:10.1038/s41587-020-0718-6.
40. Koren S, Walenz BP, Berlin K, Miller JR, Bergman NH, Phillippy AM. 2017. Canu: Scalable and accurate long-read assembly via adaptive k-mer weighting and repeat separation. *Genome Res* 27:722-736.
 41. Vaser R, Sović I, Nagarajan N, Šikić M. 2017. Fast and accurate de novo genome assembly from long uncorrected reads. *Genome Res* 27:737-746.
 42. Gurevich A, Saveliev V, Vyahhi N, Tesler G. 2013. Quast: Quality assessment tool for genome assemblies. *Bioinformatics* 29:1072-1075.
 43. Li H. 2018. Minimap2: Pairwise alignment for nucleotide sequences. *Bioinformatics* 34:3094-3100.
 44. Gatto L, Gibb S, Rainer J. 2021. MSnbase, efficient and elegant r-based processing and visualization of raw mass spectrometry data. *J Prot Res* 20:1063-1069.
 45. O'Boyle NM, Banck M, James CA, Morley C, Vandermeersch T, Hutchison GR. 2011. Open Babel: An open chemical toolbox. *J Cheminformatics* 3:33.